Time-domain modeling of dispersive and lossy liquid-crystals for terahertz applications

D. C. Zografopoulos,[1,*] K. P. Prokopidis,[2] R. Dąbrowski,[3] and R. Beccherelli[1]

[1]*Consiglio Nazionale delle Ricerche, Istituto per la Microelettronica e Microsistemi (CNR-IMM), Roma 00133, Italy*

[2]*Department of Electrical and Computer Engineering, Aristotle University of Thessaloniki, Thessaloniki GR-54124, Greece*

[3]*Institute of Chemistry, Military University of Technology, ul. gen. Kaliskiego 2, 00-908 Warsaw, Poland*

[*]*dimitrios.zografopoulos@artov.imm.cnr.it*

Abstract: A numerical framework based on the finite-difference time-domain method is proposed for the rigorous study of electro-optically tunable terahertz devices based on liquid crystals. The formulation accounts for both the liquid-crystal full-tensor anisotropy and the dispersion of its complex refractive indices, which is described via modified Lorentzian terms. Experimentally characterized liquid-crystalline materials in the terahertz spectrum are fitted and modeled in benchmark examples, directly compared with reference analytical or semi-analytical solutions. In addition, the efficiency of broadband time-domain modeling of the proposed technique is also demonstrated by accurately reproducing time-domain spectroscopy measurements.

OCIS codes: (160.3710) Liquid crystals; (300.6495) Spectroscopy, terahertz; (050.1755) Computational electromagnetic methods; (260.2030) Dispersion; (160.4760) Optical properties.

References and links

1. L. Yun-Shik, *Principles of Terahertz Science and Technology* (Springer, 2008).
2. E.R. Mueller, "Terahertz radiation sources for imaging and sensing applications," Photon. Spectra **40**, 60–69 (2006).
3. D. C. Zografopoulos, R. Asquini, E. E. Kriezis, A. d'Alessandro, and R. Beccherelli, "Guided-wave liquid-crystal photonics," Lab Chip **12**, 3598–3610 (2012).
4. D. C. Zografopoulos and R. Beccherelli, "Long-range plasmonic directional coupler switches controlled by nematic liquid crystals," Opt. Express **21**, 8240–8250 (2013).
5. D. C. Zografopoulos and R. Beccherelli, "Design of a vertically coupled liquid-crystal long-range plasmonic optical switch," Appl. Phys. Lett. **102**, 101103 (2013).
6. N. Vieweg, C. Jansen, and M. Koch, "Liquid crystals and their applications in the THz frequency range," in "Terahertz spectroscopy and imaging," vol. 171 of *Springer Series in Optical Sciences*, K.-E. Peiponen, A. Zeitler, and M. Kuwata-Gonokami, eds. (Springer, 2013), pp. 301–326.
7. N. Vieweg, M. K. Shakfa, B. Scherger, M. Mikulics, and M. Koch, "THz properties of nematic liquid crystals," J. Infrared Milli. Terahz. Waves **31**, 1312–1320 (2010).
8. H. Park, E. P. J. Parrott, F. Fan, M. Lim, H. Han, V. G. Chigrinov, and E. Pickwell-MacPherson, "Evaluating liquid crystal properties for use in terahertz devices," Opt. Express **20**, 11899–11905 (2012).
9. U. Chodorow, J. Parka, and O. Chojnowska, "Liquid crystal materials in THz technologies," Photon. Lett. Poland **4**, 112–114 (2012).

#202086 - $15.00 USD Received 26 Nov 2013; revised 13 Dec 2013; accepted 13 Dec 2013; published 10 Feb 2014

10. M. Reuter, K. Garbat, N. Vieweg, B. M. Fischer, R. Dąbrowski, M. Koch, J. Dziaduszek, and S. Urban, "Terahertz and optical properties of nematic mixtures composed of liquid crystal isothiocyanates, fluorides and cyanides," J. Mater. Chem. **1**, 4457–4463 (2013).
11. M. Reuter, N. Vieweg, B. M. Fischer, M. Mikulicz, M. Koch, K. Garbat, and R. Dąbrowski, "Highly birefringent, low-loss liquid crystals for terahertz applications," APL Mater. **1**, 012107 (2013).
12. C.-F. Hsieh, R.-P. Pan, T.-T. Tang, H.-L. Chen, and C.-L. Pan, "Voltage-controlled liquid-crystal terahertz phase shifter and quarter-wave plate," Opt. Lett. **31**, 1112–1114 (2006).
13. C.-F. Hsieh, Y.-C. Lai, R.-P. Pan, and C.-L. Pan, "Polarizing terahertz waves with nematic liquid crystals," Opt. Lett. **33**, 1174–1176 (2008).
14. S. A. Jewell, E. Hendry, T. H. Isaac, and J. R. Sambles, "Tuneable Fabry-Perot etalon for terahertz radiation," New J. Phys. **10**, 033012 (2008).
15. T. Kumagai, R. Ito, K. Takeya, H. Yoshida, H. Kubo, A. Fujii, T. Nose, M. Tonouchi, and M. Ozaki, "Tunable terahertz filter using an etalon with a nematic liquid crystal layer and its response speed," Mol. Cryst. Liq. Cryst. **561**, 82–88 (2012).
16. C.-J. Lin, C.-H. Lin, Y.-T. Li, R.-P. Pan, and C.-L. Pan, "Electrically controlled liquid crystal phase grating for terahertz waves," IEEE Photon. Technol. Lett. **21**, 730–732 (2009).
17. H. Li, C. Zhu, K. Liu, X. Zhang, F. Ling, T. Zhang, X. Shen, C. Zhang, and S. Ruan, "Terahertz electrically controlled nematic liquid crystal lens," Infrared Phys. Tech. **54**, 439–444 (2011).
18. B. Scherger, M. Reuter, M. Scheller, K. Altmann, N. Vieweg, R. Dąbrowski, J. A. Deibel, and M. Koch, "Discrete terahertz beam steering with an electrically controlled liquid crystal device," J. Infrared Milli. Terahz. Waves **33**, 1117–1122 (2012).
19. C.-L. Chang, W.-C. Wang, H.-R. Lin, F. J. Hsieh, Y.-B. Pun, and C.-H. Chan, "Tunable terahertz fishnet metamaterial," Appl. Phys. Lett. **102**, 151903 (2013).
20. D. Shrekenhamer, W.-C. Chen, and W. J. Padilla, "Liquid crystal tunable metamaterial absorber," Phys. Rev. Lett. **110**, 177403 (2013).
21. A. Taflove and S. C. Hagness, *Computational Electrodynamics: The Finite-Difference Time-Domain Method*, 3rd ed., (Artech House, 2005).
22. N. Wongkasem, A. Akyurtlu, J. Li, A. Tibolt, Z. Kang, and W. D. Goodhue, "Novel broadband terahertz negative refractive index metamaterials: analysis and experiment," Prog. Electromagn. Res. **64**, 205–218 (2006).
23. L. Dou and A. R. Sebak, "3D FDTD method for arbitrary anisotropic materials," Microw. Opt. Techn. Let. **48**, 2083–2090 (2006).
24. E. E. Kriezis and S. J. Elston, "Light wave propagation in liquid crystal displays by the 2-D finite-difference time-domain method," Opt. Commun. **177**, 69–77 (2000).
25. M. N. Miskiewicz, P. T. Bowen, and M. J. Escuti, "Efficient 3D FDTD analysis of arbitrary birefringent and dichroic media with obliquely incident sources," Proc. SPIE **8255**, 82550W (2012).
26. G. Gilardi, D. Donisi R. Beccherelli, and A. Serpengüzel, "Liquid crystal tunable filter based on sapphire microspheres," Opt. Lett. **34**, 3253–3255 (2009).
27. D. Donisi, B. Bellini, R. Beccherelli, R. Asquini, G. Gilardi, M. Trotta, and A. d'Alessandro, "A switchable liquid-crystal optical channel waveguide on silicon," IEEE J. Quantum Electron. **46**, 762–768 (2010).
28. K. P. Prokopidis, D. C. Zografopoulos, and E. E. Kriezis, "Rigorous broadband investigation of liquid-crystal plasmonic structures using FDTD dispersive-anisotropic models," J. Opt. Soc. Am. B **30**, 2722–2730 (2013).
29. A. Deinega and S. John, "Effective optical response of silicon to sunlight in the finite-difference time-domain method," Opt. Lett. **37**, 112–114 (2012).
30. A. Vial, T. Laroche, M. Dridi, and L. Le Cunff, "A new model of dispersion for metals leading to a more accurate modeling of plasmonic structures using the FDTD method," Appl. Phys. A: Mater. Sci. Process. **103**, 849–853 (2011).
31. U. Chodorow, J. Parka, K. Garbat, N. Palka, and K. Czupryński, "Spectral investigation of nematic liquid crystals with high optical anisotropy at THz frequency range," Phase Transit. **85**, 337–344 (2012).
32. I. Pupeza, R. Wilk, and M. Koch, "Highly accurate optical material parameter determination with THz time-domain spectroscopy," Opt. Express **15**, 4335–4350 (2007).
33. R. Wilk, I. Pupeza, R. Cernat, and M. Koch, "Highly accurate THz time-domain spectroscopy of multilayer structures," IEEE J. Select. Top. Quant. Electron. **14**, 392–398 (2008).
34. J. Li, C.-H. Wen, S. Gauza, R. Lu, and S.-T. Wu, "Refractive indices of liquid crystals for display applications," J. Display Technol. **1**, 51–61 (2005).
35. A. Vial and T. Laroche, "Description of dispersion of metals by means of the critical points model and application to the study of resonant structures using the FDTD method," J. Phys. D: Appl. Phys. **40**, 7152–7158 (2007).
36. K. P. Prokopidis and D. C. Zografopoulos, "A unified FDTD/PML scheme based on critical points for accurate studies of plasmonic structures," J. Lightwave Technol. **31**, 2467–2476 (2013).
37. N. Vieweg, M. Shakfa, and M. Koch, "BL037: A nematic mixture with high terahertz birefringence," Opt. Commun. **284**, 1887–1889 (2011).
38. O. Chojnowska and R. Dąbrowski, "The influence of cyano compound on liquid crystal blue phase range," Photon. Lett. Poland **4**, 81–83 (2012).

#202086 - $15.00 USD Received 26 Nov 2013; revised 13 Dec 2013; accepted 13 Dec 2013; published 10 Feb 2014

39. MATLAB Release 2012b, The MathWorks, Inc., Natick, Massachusetts, USA (www.mathworks.com).
40. I.-C. Khoo, *Liquid Crystals*, 2nd ed., (Wiley, 2007).
41. D. W. Berreman, "Liquid-crystal twist cell dynamics with backflow," J. Appl. Phys. **46**, 3746–3751 (1975).
42. J. A. Roden and S. D. Gedney, "Convolution PML (CPML): An efficient FDTD implementation of the CFS-PML for arbitrary media," Microw. Opt. Techn. Lett. **27**, 334–339 (2000).
43. N. Vieweg, B. M. Fischer, M. Reuter, P. Kula, R. Dabrowski, M. A. Celik, G. Frenking, M. Koch, and P. U. Jepsen, "Ultrabroadband terahertz spectroscopy of a liquid crystal," Opt. Express **20**, 28249–28256 (2012).

1. Introduction

A rapidly growing research interest has been focused lately on the scientific field of terahertz (THz) technology, which deals with the electromagnetic (EM) properties of materials and devices in the so-called THz gap, *i.e.*, the spectral window that links the more extensively investigated microwave and infrared (IR) frequencies. A broad range of novel applications is envisaged, based on material properties that are particular to this spectral region. These infiltrate numerous scientific fields, spanning from chemical detection of explosives or other hazardous materials, safe bio-imaging and detection of diseases, to inherently secure short-range communications and non-destructive testing in industry [1].

For these advances to reach technological maturity, the necessary instrumentation for the generation, manipulation, and detection of THz waves is indispensable. Apart from sources and detectors [2], the extensive functionalities required for the development of high-end systems typically demand for a number of components, such as modulators, switches and filters, whose properties are dynamically tuned by means of an external control signal. In this context, liquid crystalline (LC) materials offer a traditional ultra-low power consumption solution, which has been thus far widely explored and demonstrated in the field of tunable optics, photonics, and plasmonics [3–5]. Their large dielectric anisotropy and their response to applied electric or magnetic fields provide a direct means to dynamically control the refractive and polarization properties of LC-infiltrated elements. These favorable properties are also present in the THz spectrum, stimulating research on both advanced LC materials and technology [6]. Indeed, a whole range of THz tunable components, based on the use of both traditional and novel highly-birefringent and low-loss LC materials [7–11], has been already demonstrated, such as tunable waveplates and polarizers [12,13], filters [14,15], gratings [16], lenses [17], beam-steerers [18], and metamaterials [19, 20].

As it is not always possible to identify analytical solutions, the design and investigation of advanced THz components demands for numerical tools, capable of capturing the EM properties of materials and structures particular to this spectral region. The finite-difference time-domain (FDTD) method is an established and efficient numerical tool for the broadband characterization of EM devices ranging from the microwave to the visible (VIS) frequencies [21] and it has also been successfully implemented for the analysis of advanced THz structures, *e.g.*, metamaterials [22]. When LCs come into play, the FDTD method can be extended in order to include material anisotropy [23] and it can be properly adjusted for the simulation of non-dispersive LC materials [24, 25]. Nevertheless, contrary to the VIS/IR spectrum, where typically a few-μm LC-infiltrated cells and cavities are employed [26, 27], the rigorous investigation LC-THz components needs to take into account both the material absorption losses, which often show strong dichroism, and the dispersion of the LC refractive indices in the broad THz spectrum.

Recently, some of us have introduced an auxiliary differential equation (ADE) FDTD dispersive/anisotropic formulation, which models the LC index dispersion via Lorentzian terms. It was shown that the formulation is capable of describing the LC dispersive properties in the VIS/IR [28]. In this work, we extend the FDTD scheme by modeling the LC dielectric properties via modified Lorentz (m-Lor) terms, a generalized function of dispersion that encompasses as subcases the well-known Debye, Drude, and Lorentz models. The m-Lor model provides

#202086 - $15.00 USD Received 26 Nov 2013; revised 13 Dec 2013; accepted 13 Dec 2013; published 10 Feb 2014

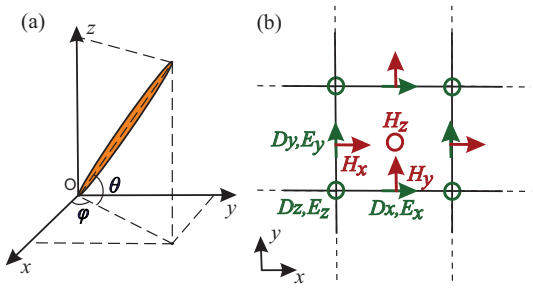

Fig. 1. (a) The local LC orientation is described by the nematic molecular director, which is defined via the spatially dependent tilt (θ) and twist (φ) angles. (b) Unit cell employed in the proposed FDTD formulation.

extensive degrees of freedom in terms of representing phenomenologically the complex index dispersion of experimentally characterized LC materials, as it was recently demonstrated in the case of isotropic metals and semiconductors [29, 30]. In this work, the complex dispersion of both reference [7, 8] and novel experimentally characterized [9, 31] LC-THz materials is fitted to the m-Lor model, successfully describing their dielectric properties. The proposed formulation is tested and validated in two benchmark examples, transmission through a LC-slab placed between crossed-polarizers and a LC-tunable Fabry-Pérot filter, which have analytical and semi-analytical solutions, respectively. In addition, time-domain spectroscopy (TDS) [1, 32, 33] experimental measurements of THz pulse propagation through LC cells are reproduced numerically, demonstrating the effectiveness of the proposed formulation in the broadband investigation of LC-THz structures.

2. Time-domain modeling of THz liquid-crystals via modified Lorentzian terms

The local molecular orientation of nematic LC materials with an arbitrary spatial alignment profile is described via the nematic director, a unit vector defined via the tilt θ and twist ϕ angles, as shown in Fig. 1(a). The local orientation directly impacts on the LC anisotropic EM properties, which are described via the relative permittivity tensor $\tilde{\varepsilon}$ [24, 28]

$$\tilde{\varepsilon} = \begin{pmatrix} \varepsilon_o + \Delta\varepsilon\cos^2\theta\cos^2\phi & \Delta\varepsilon\cos^2\theta\sin\phi\cos\phi & \Delta\varepsilon\sin\theta\cos\theta\cos\phi \\ \Delta\varepsilon\cos^2\theta\sin\phi\cos\phi & \varepsilon_o + \Delta\varepsilon\cos^2\theta\sin^2\phi & \Delta\varepsilon\sin\theta\cos\theta\sin\phi \\ \Delta\varepsilon\sin\theta\cos\theta\cos\phi & \Delta\varepsilon\sin\theta\cos\theta\sin\phi & \varepsilon_o + \Delta\varepsilon\sin^2\theta \end{pmatrix}, \tag{1}$$

where ε_o and ε_e are the complex ordinary and extraordinary LC relative dielectric constants, respectively, and $\Delta\varepsilon = \varepsilon_e - \varepsilon_o$ is the LC relative dielectric anisotropy.

In the following, focusing on the case where the optical axis of the LC lies in the $x-y$ plane ($\theta = 0$), the frequency-dependent non-negative elements of the relative permittivity tensor are given by

$$\begin{aligned} \varepsilon_{xx}(\omega) &= \varepsilon_o(\omega) + [\varepsilon_e(\omega) - \varepsilon_o(\omega)]\cos^2\phi, \\ \varepsilon_{yy}(\omega) &= \varepsilon_o(\omega) + [\varepsilon_e(\omega) - \varepsilon_o(\omega)]\sin^2\phi, \\ \varepsilon_{xy}(\omega) &= \varepsilon_{yx}(\omega) = [\varepsilon_e(\omega) - \varepsilon_o(\omega)]\sin\phi\cos\phi, \\ \varepsilon_{zz}(\omega) &= \varepsilon_o(\omega). \end{aligned} \tag{2}$$

According to the constitutive relation $\mathbf{D}(\omega) = \varepsilon_0\tilde{\varepsilon}(\omega)\mathbf{E}(\omega)$, ε_0 being the vacuum permittivity, the components of the dielectric displacement $\mathbf{D}$ are given by

$$D_x = \varepsilon_0[\varepsilon_o(\omega)\sin^2\phi + \varepsilon_e(\omega)\cos^2\phi]E_x + \varepsilon_0[\varepsilon_e(\omega) - \varepsilon_o(\omega)]\sin\phi\cos\phi E_y, \tag{3}$$

#202086 - $15.00 USD Received 26 Nov 2013; revised 13 Dec 2013; accepted 13 Dec 2013; published 10 Feb 2014

$$D_y = \varepsilon_0[\varepsilon_e(\omega) - \varepsilon_o(\omega)]\sin\phi\cos\phi\, E_x + \varepsilon_0[\varepsilon_o(\omega)\cos^2\phi + \varepsilon_e(\omega)\sin^2\phi]\, E_y, \tag{4}$$

$$D_z = \varepsilon_0\varepsilon_o(\omega)\, E_z. \tag{5}$$

Equations (3) and (4) are reformulated by introducing eight auxiliary variables, in order to separate the x and y components of the electric field,

$$W_{x1} = \varepsilon_0\varepsilon_o(\omega)\sin^2\phi E_x,\ \ W_{x2} = \varepsilon_0\varepsilon_e(\omega)\cos^2\phi\, E_x, \tag{6}$$

$$W_{y1} = \tfrac{1}{2}\varepsilon_0\varepsilon_e(\omega)\sin(2\phi)E_y,\ \ W_{y2} = -\tfrac{1}{2}\varepsilon_0\varepsilon_o(\omega)\sin(2\phi)E_y, \tag{7}$$

$$R_{x1} = \tfrac{1}{2}\varepsilon_0\varepsilon_e(\omega)\sin(2\phi)E_x,\ \ R_{x2} = -\tfrac{1}{2}\varepsilon_0\varepsilon_o(\omega)\sin(2\phi)E_x, \tag{8}$$

$$R_{y1} = \varepsilon_0\varepsilon_o(\omega)\cos^2\phi\, E_y,\ \ R_{y2} = \varepsilon_0\varepsilon_e(\omega)\sin^2\phi E_y. \tag{9}$$

where $D_x = W_{x1} + W_{x2} + W_{y1} + W_{y2}$ and $D_y = R_{x1} + R_{x2} + R_{y1} + R_{y2}$. In the present case, where the optical axis lies in the $x-y$ plane, the D_z component can be handled as in the case of isotropic media. The position of the EM fields components in the FDTD grid are shown in the unit cell of Fig. 1(b).

In [28] the Lorentz model was chosen for the frequency description of the dielectric tensor elements, which is sufficient for the accurate description of LC index dispersion in the VIS/IR, typically described by the Cauchy model [34]. Nevertheless, in the THz spectrum the LC dispersion depends strongly on the material chemical composition and molecular resonances and, in general, it cannot be described by simple analytical models. Moreover, LC-THz materials show strong dichroism and, contrary to VIS/IR LC-based applications, the absorption losses along both the ordinary and the extraordinary axes must be taken rigorously into account. To this end, the description of $\varepsilon_{o/e}(\omega)$ is here modeled via m-Lor terms. It has been shown that the m-Lor analytical function can provide higher quality broadband fitting to experimentally measured permittivity values for many isotropic materials such as silicon [29] and noble metals [35, 36], while it can be proved that it satisfies the Kramers-Kronig relations. Following the proposed formulation, the LC permittivities are expressed as

$$\varepsilon_{o/e}(\omega) = \varepsilon_{\infty,o/e} + \frac{a_{1,o/e}\, j\omega + a_{0,o/e}}{b_{2,o/e}(j\omega)^2 + b_{1,o/e}\, j\omega + b_{0,o/e}}, \tag{10}$$

where the parameters a_i and b_i can be calculated through a fitting algorithm of available data.

It can be observed in (6)-(9) that the auxiliary variables $W_{\bullet}$ and $R_{\bullet}$ obey the differential equation of a m-Lor medium, involving the dispersive function of either $\varepsilon_o(\omega)$ or $\varepsilon_e(\omega)$, which is multiplied with non-dispersive sine/cosine coefficients. The differential equation of W_{x1}, for instance, is discretized using central finite differences of second-order accuracy

$$\begin{aligned}&\left(b_{2,o}\frac{\delta_t^2}{\Delta t^2} + b_{1,o}\frac{\mu_t\delta_t}{\Delta t} + b_{0,o}\mu_t^2\right) W_{x1}^n = \\ &\varepsilon_0\sin^2\phi\left(\varepsilon_{\infty,o}b_{2,o}\frac{\delta_t^2}{\Delta t^2} + (a_{1,o} + b_{1,o}\varepsilon_{\infty,o})\frac{\mu_t\delta_t}{\Delta t} + (a_{0,o} + b_{0,o}\varepsilon_{\infty,o})\mu_t^2\right)E_x^n,\end{aligned} \tag{11}$$

leading to the following update equation for the variable P_{x1}

$$W_{x1}^{n+1} = \frac{1}{c_{o1}}\left(c_{o4}\sin^2\phi\, E_x^{n+1} + c_{o5}\sin^2\phi\, E_x^n + c_{o6}\sin^2\phi\, E_x^{n-1} - c_{o2}\, W_{x1}^n - c_{o3}\, W_{x1}^{n-1}\right), \tag{12}$$

#202086 - $15.00 USD Received 26 Nov 2013; revised 13 Dec 2013; accepted 13 Dec 2013; published 10 Feb 2014

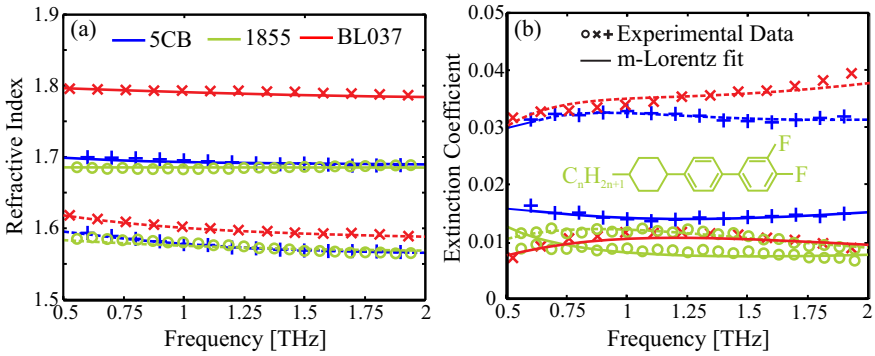

Fig. 2. Experimentally measured and m-Lor fitted values of (a) refractive index and (b) extinction coefficient of the three reference LC materials used in this study, *i.e.*, 5CB [7], BL037 [8], and the low-loss mixture of fluorinated biphenyls 1855 [9, 38]. Markers denote experimental values, continuous and dashed lines denote fitted extraordinary and ordinary index values, respectively. The inset in (b) shows the molecular structure of the three constituent molecules of 1855 ($n = 2, 3, 5$).

where the coefficients c_{oi}, $i = 1, \ldots, 6$ are given by

$$
\begin{aligned}
c_{o1} &= \frac{b_{0,o}}{4} + \frac{b_{1,o}}{2\Delta t} + \frac{b_{2,o}}{\Delta t^2}, \quad c_{o2} = \frac{b_{0,o}}{2} - \frac{2b_{2,o}}{\Delta t^2}, \quad c_{o3} = \frac{b_{0,o}}{4} - \frac{b_{1,o}}{2\Delta t} + \frac{b_{2,o}}{\Delta t^2}, \\
c_{o4} &= \varepsilon_0 \left(\frac{a_{0,o} + \varepsilon_{\infty,o} b_{0,o}}{4} + \frac{a_{1,o} + b_{1,o}\varepsilon_{\infty,o}}{2\Delta t} + \frac{\varepsilon_{\infty,o} b_{2,o}}{\Delta t^2} \right), \\
c_{o5} &= \varepsilon_0 \left(\frac{a_{0,o} + \varepsilon_{\infty,o} b_{0,o}}{2} - \frac{2\varepsilon_{\infty,o} b_{2,o}}{\Delta t^2} \right), \\
c_{o6} &= \varepsilon_0 \left(\frac{a_{0,o} + \varepsilon_{\infty,o} b_{0,o}}{4} - \frac{a_{1,o} + b_{1,o}\varepsilon_{\infty,o}}{2\Delta t} + \frac{\varepsilon_{\infty,o} b_{2,o}}{\Delta t^2} \right).
\end{aligned}
\tag{13}
$$

Similar equations can be obtained for the other auxiliary variables. Using the update equations of $\boldsymbol{W}_\bullet$, a difference equation for D_x^{n+1} can be obtained. The difference equation for D_y^{n+1} derives similarly from the update equations of the $\boldsymbol{R}_\bullet$ variables. Finally, the update expressions of E_x^{n+1} and E_y^{n+1} are calculated by solving the 2×2 system of linear equations that involve D_x and D_y, as described in extent in [28]. It is stressed that the extension of the classical Lorentz model ($a_1 = 0$) in the proposed implementation comes at no cost in terms of auxiliary variables and, therefore, memory requirements.

3. Numerical results and discussion

In this section, the accuracy of the proposed methodology is validated by investigating LC-THz structures based on three benchmark LC materials, the well known single molecule cyanobiphenyl 5CB [7], the highly birefringent nematic mixture BL037 [8, 37] and the material 1855, an in-house synthetized low-loss mixture of fluorinated biphenyls [9, 38], whose molecular structure is shown in the inset of Fig. 2(b). The dielectric properties of these LCs are described by their complex index of refraction $\tilde{n}_{o/e} = n_{o/e} - jk_{o/e}$, where $n_{o/e}$ is the refractive index and $k_{o/e}$ the absorption coefficient. Nematic LC-THz materials are both dispersive and dichroic, which means that the accurate modeling of their properties depends on the fitting of the four functions $n_{o/e}(\lambda)$ and $k_{o/e}(\lambda)$. Here, using the data provided in [7–9], the experimental values are fitted in the $0.5 - 2$ THz window to a m-Lor term via the nonlinear optimization

#202086 - $15.00 USD Received 26 Nov 2013; revised 13 Dec 2013; accepted 13 Dec 2013; published 10 Feb 2014

Nelder-Mead technique implemented in the `fminsearch` function of Matlab© [39], making use of the known expressions $\Re\{\varepsilon\} = n^2 - k^2$ and $\Im\{\varepsilon\} = 2nk$. The fitted parameter values for the ordinary and extraordinary permittivities of the three LC materials are summarized in Table 1 and a comparison between the experimental data and the fitted functions is shown in Fig. 2. A single m-Lor term is sufficient to capture the dispersive behavior of both the refractive index and the absorption coefficient, despite the fact that their functions show different trends. It is pointed out that the fitted parameters of Table 1 are not necessarily associated with the physical properties of the LC materials, but they provide an analytical description of their permittivity dispersion, in the context of the time-domain studies of LC-THz structures.

Figure 3 shows a direct comparison between measured data [9] on the characterization of the mixture 1855 and a FDTD simulation of the experimental setup, using the fitted m-Lor model parameters of Table 1 and the formulation presented in Section 2. The LC was characterized using a standard TDS technique [1]. A 0.5-mm LC layer was sandwiched between two 1.5-mm quartz plates LC cells, modeled with an index $n_g = 1.95$. Copper wires as separators and electrodes were used, and a homogeneous LC alignment was obtained by applying a high voltage of about 30 kV/m. In this work, the reference signal was transmitted through two directly-adjacent quartz plates, and it was used as the FDTD excitation. The application of a fast Fourier transform (FTT) on the reference and the transmitted signal yields their complex transmission coefficients $T(\omega)$, whose amplitude and phase contains the information on the LC complex indices, as described in detail in [31]. The model here proposed accurately reproduces both the retardation, directly linked to the refractive indices $n_{o/e}$ and the attenuation of the THz pulse, which stems from the material absorption given by $k_{o/e}$. The FDTD parameters used were a spatial step $\Delta z = 0.5$ μm, and time-step $\Delta t = 0.8\Delta z/c$, where c is the speed of light in vacuum.

As a next case example, we study EM wave propagation through a LC layer placed between crossed polarizers as in the inset of Fig. 4. The analytical expression for the transmittance through the layer is given by

$$T(f) = 0.25\sin^2(2\varphi)\left|e^{-j[n_e(f)-jk_e(f)]k_0 d} - e^{-j[n_o(f)-jk_o(f)]k_0 d}\right|^2, \tag{14}$$

where $k_0 = 2\pi f/c$ and d the thickness of the slab. In the lossless case ($k_{o/e} = 0$), the expression (14) reduces to the known formula [40]

$$T(f) = \sin^2(2\varphi)\sin^2\left[\frac{\pi d f \Delta n(f)}{c}\right], \tag{15}$$

where $\Delta n(f) = n_e(f) - n_o(f)$ is the LC birefringence at frequency f. The LC slab thickness is $d = 1.5$ mm and the LC twist angle $\varphi = 45^\circ$. The transmittance is calculated for the three reference LC materials and FDTD results are compared with the analytical solutions corresponding

Table 1. Fitted m-Lor parameters for the ordinary (o) and extraordinary (e) permittivities of the three LC materials under study in the $0.5 - 2$ THz spectral window.

LC	ε_∞	a_0	a_1 [ps]	b_0	b_1 [ps]	b_2 [ps^2]
5CB (o)	2	1.2622	0.2148	2.0746	0.5015	0.0041
5CB (e)	2.4	3.3539	1.1795	6.1051	2.616	0.0156
BL037 (o)	1.85	12.181	2.3726	14.6175	3.6541	0.03
BL037 (e)	2.272	1.7127	0.21	1.7621	0.2343	0
1855 (o)	2.2	2.7662	0.3871	8.3725	1.5355	0
1855 (e)	2.5	9.5127	26.8743	0	77.921	0.3053

#202086 - $15.00 USD Received 26 Nov 2013; revised 13 Dec 2013; accepted 13 Dec 2013; published 10 Feb 2014

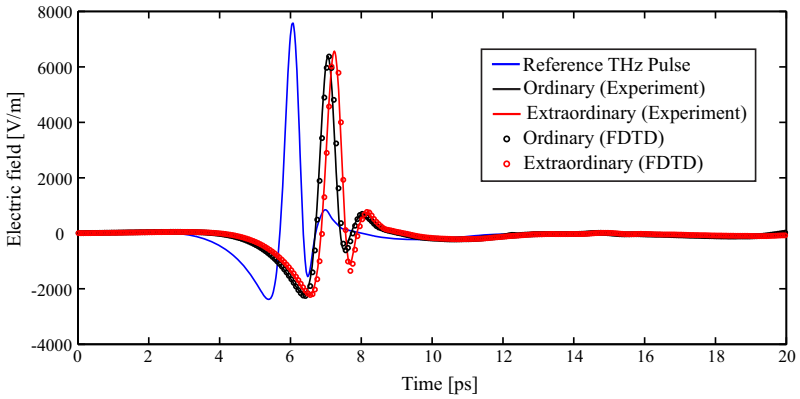

Fig. 3. Measured THz pulse waveforms for the experimental characterization of the LC mixture 1855 [9] and FDTD simulations using the m-Lor fitted values of Table 1.

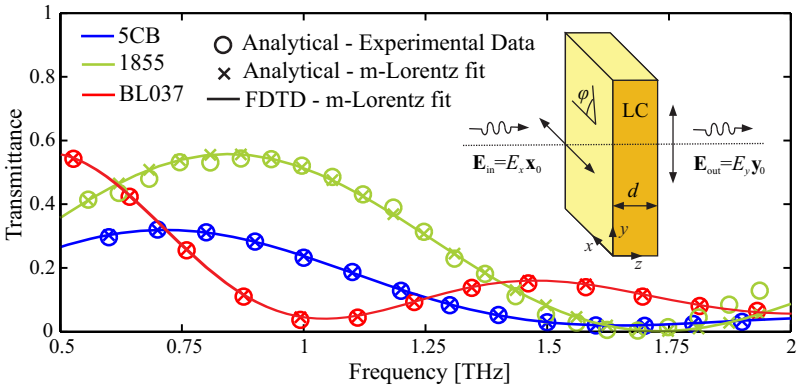

Fig. 4. Transmittance of a LC slab between cross polarizers calculated by the proposed method for the three reference LC materials. Results are compared with the analytic solution of both the experimentally measured LC index data and their fit to the m-Lor dispersive model. The slab thickness is $d = 1.5$ mm and the LC twist angle $\varphi = 45°$.

to both the experimental data and the fitted m-Lor functions. Figure 4 shows excellent agreement between the FDTD results and the analytical solution of the fitted function, with absolute errors below 0.001. These originate from the inherent FDTD numerical dispersion and can be further reduced by choosing a smaller spatial step Δz. Thus, the overall deviation with respect to the reference results, which were calculated using the experimental values, are attributed to the fitting quality of experimental data to the m-Lor function, and not the FDTD implementation.

Finally, the properties of the LC-tunable Fabry-Pérot filter shown in the Fig. 5(a) are investigated via the proposed method and compared to the semi-analytical solution provided by the 4×4 Berreman matrix method [41]. The reflective mirrors of the filter are composed of alternating layers of glass and air, whose thickness is matched for a central bandgap frequency of 1 THz, namely $d_a = 75$ µm and $d_g = 38.5$ µm, for refractive index values equal to $n_a = 1$ and $n_g = 1.95$. The resonant cavity is a 150-µm layer of the LC material 1855, with a uniform alignment in the $x-y$ plane described by the twist angle φ between the director and the x-axis. The simulation parameters used were $\Delta z = 0.5$ µm, $\Delta t = 0.8\Delta z/c$, and the computational domain was backed by a 12-cell convolution perfectly matched layer for the efficient absorption

#202086 - $15.00 USD Received 26 Nov 2013; revised 13 Dec 2013; accepted 13 Dec 2013; published 10 Feb 2014

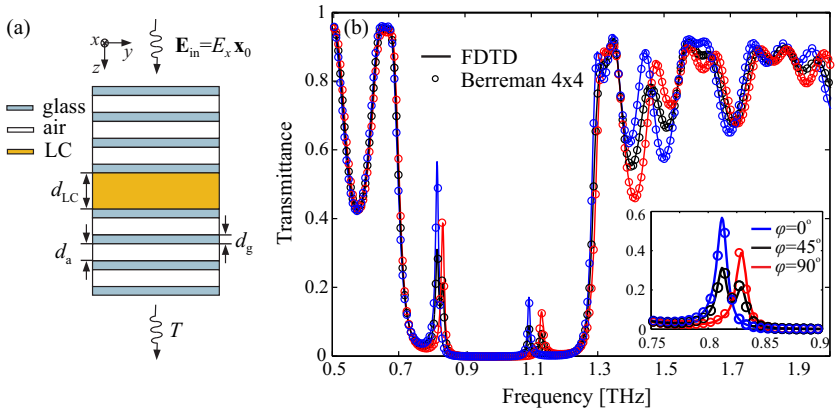

Fig. 5. Transmittance of a LC-THz Fabry-Pérot filter calculated via the Berreman 4×4 method and the proposed formulation. The reflective mirror is composed of alternating slabs of glass ($d_g = 38.5$ µm, $n_g = 1.95$) and air ($d_a = 75$ µm, $n_a = 1$). The resonant cavity of thickness $d_{\mathrm{LC}} = 150$ µm is infiltrated with the LC mixture 1855, whose director lies in the $x-y$ plane at a fixed angle φ with the x-axis.

of outgoing waves [42]. The FDTD domain was excited by a modulated Gaussian pulse with spectral content in the region from 150 µm to 600 µm.

The filter shows two resonant defect modes within the bandgap at approximately 0.8 and 1.1 THz, whose spectral position depends on the LC twist angle, as in the inset of Fig. 5. When $\varphi = 45^\circ$ the resonance splits in two defect modes, stemming from the filter's response to the two orthogonal polarizations of the impinging THz wave, which undergoes polarization rotation while passing through the LC slab. The reference solution is calculated for the experimental index values and it is juxtaposed with the numerical simulation of the fitted LC material. The FDTD model is shown to predict the semi-analytical results with very good accuracy. Again, it has been verified that the small degree of disagreement, found less than 1%, is due to the fitting error of the LC indices. This error can be minimized by using more advanced fitting techniques and/or reducing the noise of the fitted experimental samples. Furthermore, in case the ultra-broadband modeling of LC materials is targeted, where multiple resonances are expected [43], the fitting can be optimized by using additional m-Lor terms, albeit at the cost of increased algorithm complexity and memory requirements to store the additional auxiliary variables.

4. Conclusions

In conclusion, a numerical technique has been presented for the rigorous time-domain analysis of LC-based THz structures, which takes into account the dispersive properties of both the refractive indices and the absorption coefficients of LC materials in the THz spectrum. The fitting parameters for three reference LC materials are provided and numerical studies validate the accuracy of the proposed model in reference LC-tunable THz components. Furthermore, experimental measurements of the time-domain spectroscopy characterization of THz-LC are accurately reproduced, thus demonstrating the efficiency of the presented method as a numerical tool for the broadband investigation of LC-THz devices.

Acknowledgments

This work was financially supported by the Italian Ministry of Foreign Affairs, Directorate General for the Country Promotion, and by the projects PBS 847.

#202086 - $15.00 USD Received 26 Nov 2013; revised 13 Dec 2013; accepted 13 Dec 2013; published 10 Feb 2014